Mechanism and Machine Theory 44 (2009) 1826–1839

Contents lists available at ScienceDirect

Mechanism and Machine Theory

journal homepage: www.elsevier.com/locate/mechmt

Optimized flexural hinge shapes for microsystems and high-precision applications

Saša Zelenika [a,b,*], Mircea Gh. Munteanu [b], Francesco De Bona [b]

[a] University of Rijeka, Faculty of Engineering, Department of Mechanical Engineering Design, Vukovarska 58, 51000 Rijeka, Croatia
[b] University of Udine, DIEGM, Via delle Scienze 208, 33100 Udine, Italy

ARTICLE INFO

Article history:
Received 22 April 2008
Accepted 20 March 2009
Available online 29 April 2009

Keywords:
Microsystems
High precision
Compliant mechanisms
Flexural hinges
Shape optimization
Parametric FEM model
Design guidelines

ABSTRACT

Positioning devices based on flexural hinges are often used in microsystems and precision mechanisms. In this work a nonlinear parametric optimization of flexural hinge shapes is performed. Predefined and freeform parametric shapes are compared in terms of compliance, strength, stress concentration factors and parasitic shifts. Transversal and axial compliances and stress concentration factors are also calculated, permitting design guidelines to be established. It is shown that optimized hinge shapes lead to far better performances with respect to conventional circular notches.

1. Introduction

The design of mechanical devices for application in information technology, metrology, robotics, in the field of microsystems (cantilevers, sensors, metrology devices, etc.), but also in particle accelerators (e.g. optics manipulation units), in precision machine tools, as well as in other applications, often makes use of compliant mechanisms relying on the elastic properties of matter [1–6]. These devices are often based on the employment of flexural hinges [7,8] where the primary (also referred to as sensitive) degree of freedom (DOF) is rotation ϕ_z around a single bending axis (Fig. 1). High off-axis stiffness minimizes deformations along these DOFs. Flexures-based design makes possible the attainment of monolithic microdevices (i.e. where no assembly is needed) characterized by compatibility with the respective working environments (e.g. clean room micro-fabrication facilities, vacuum or radiation environments), as well as the attainment of frictionless ultra-high precision positioning on the meso- and macro-scale [3,5,7–15].

Until recently the choice of notch shapes for flexural hinges was determined by the available production technologies. In fact, the notches were mainly produced by conventional rotating machine tools and therefore were limited to circular shapes. The availability of high-precision milling and especially of electro-discharge machining (EDM), as well as of lithography-based micro-manufacturing technologies, has allowed these limitations to be overcome. The shapes of the notches can therefore nowadays be chosen based on the design requirements for specific applications. A strong improvement of the flexural hinge main features can thus be achieved. In particular, the main drawback of compliant mechanisms based on flexures – their limited travel ranges – can be tackled [7].

* Corresponding author. Address: University of Rijeka, Faculty of Engineering, Department of Mechanical Engineering Design, Vukovarska 58, 51000 Rijeka, Croatia. Tel.: +385 (0)51 651538; fax: +385 (0)51 651416.
E-mail address: sasa.zelenika@riteh.hr (S. Zelenika).

0094-114X/$ - see front matter © 2009 Elsevier Ltd. All rights reserved.
doi:10.1016/j.mechmachtheory.2009.03.007

Nomenclature

a	length of the hinge fillet region along the y axis; semi-axis of the elliptic hinge [m]
b	height of the hinge fillet region along the x axis; semi-axis of the elliptic hinge [m]
BS	Baud's hinge shape
C_{nrm}	normalized compliance [rad] as defined in Eq. (7)
e	eccentricity, i.e. deviation of the flexural kinematics from that of an ideal hinge [m]
E	Young's modulus [Pa]
EB	elliptic hinge having the same fillet height as the BS hinge
F	objective function in the optimization process
FO	freeform optimized hinge shape
GR	Grodzinski's hinge shape
i	index that indicates the various hinge fillet shapes
K_{C}	compliance ratio as defined in Eq. (10)
K_{δ}	relative parasitic shift amplitude as defined in Eq. (11)
K_{σ}	ratio of normalized (i.e. maximal) stresses as defined in Eq. (9)
K_{σ}^{*}	relative stress concentration factor as defined in Eq. (12)
L	hinge length [m]
L_{p}	length of the prismatic section of the hinge [m]
M	couple loading the hinge [Nm]
OC	optimized circular hinge shape
OE	optimized elliptical hinge shape
PC	pure circular hinge shape
PP'	parasitic shift [m]
PR	prismatic beam hinge
r	fillet radius in the case of circular hinge fillets [m]
r_i	radii of the middle points of the spline functions defining the FO fillet shape [m]
s	length of the hinge contour [m]
$t(y)$	hinge thickness varying along its length [m]
t_{min}	minimal hinge thickness [m]
TB	Thum's and Bautz's hinge shape
w	width of the hinge [m]
x,y	coordinate system in hinge plane
α_{k}	stress concentration factor
$\gamma = L/t_{\mathrm{min}}$	hinge aspect ratio
δ_{nrm}	normalized parasitic shift as defined in Eq. (8)
θ	slope of the tangent to the hinge fillet with respect to the x axis [rad]
σ	normal stress [Pa]
σ_{n}	nominal stress [Pa]
σ_{nrm}	normalized stress [rad^{-1}] as defined in Eq. (6)
σ_{max}	maximum stress in the hinge [Pa]
τ	tangential stress [Pa]
ϕ_{z}	primary rotation (sensitive) degree of freedom [rad]

Starting from the closed form Euler–Bernoulli beam model developed by Paros and Weisbord [16] for conventional circular hinges, several authors have hence dealt with the compliance of flexural hinges of different shapes. In particular, Smith and coauthors [17] calculated analytically and numerically the stiffness and stress concentration factors of elliptical flexural hinges with different major-to-minor axis ratios and verified experimentally the obtained results. A generalized extension of this approach by employing energy considerations was given by Lobontiu [7], where a wide range of single- and multiple-axes flexural hinge shapes (elliptic, parabolic and hyperbolic) were considered both analytically and numerically in terms of their in-plane and out-of-plane compliances; the actual hinge kinematics was also analyzed.

A compliance optimization along the sensitive DOF, based on a parametric finite element model (FEM), was recently proposed by De Bona and Munteanu [18], allowing freeform optimized hinge shapes to be obtained. Kinematics and strength constraints are considered in the optimization process. In fact, extension of the hinge range of motion along the primary DOF is coupled with the necessity to consider its behavior in the geometrically nonlinear field where parasitic deflections become clearly evident. The calculation of nonlinear effects, as well as the necessity to consider stress-concentration effects, fully justifies the employment of a numerical (FEM) approach.

From the above analysis of the state of the art it is evident that an integrated approach to the optimized design of flexural hinges, which would allow determining advantages and drawbacks of predefined and freeform hinge shapes, is still missing. In this work, therefore, the optimization procedure developed by De Bona and Munteanu [18] is revisited so as to take

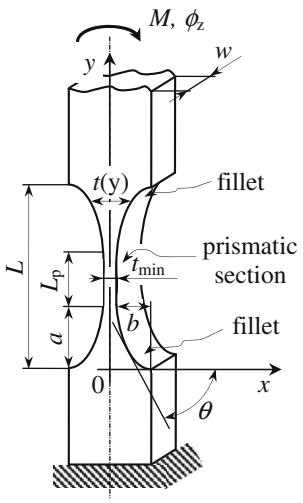

Fig. 1. Flexural hinge with parameters defining its shape.

localized effects of hinge shape modifications into account better via the objective function. The hence-obtained optimal freeform shape is compared in terms of strength, compliance and parasitic shifts to:

- predefined (circular and elliptic) shapes whose geometric parameters are chosen so as to minimize the occurring peak stresses,
- conventional shapes obtained via stress minimization criteria for shoulder fillets.

The comparison is performed for varying hinge aspect ratios $\gamma = L/t_{\min}$.

Transversal bending (out of hinge plane, i.e. around x axis shown in Fig. 1) and axial (along y axis) compliances and stress concentration factors of the considered flexural hinge shapes are also calculated. Transversal compliance is important in applications where, due to micro-fabrication technologies, the distance between the suspended moving platform and the respective substrate is limited. Insufficient stiffness can thus lead to stiction problems. Axial compliance is particularly relevant for slender hinges, as here axial and flexural behavior can be coupled. This compliance can also influence the positioning precision significantly.

Generalized design guidelines taking into account the hinge shape, geometrical and technological constrains, compliance, strength, parasitic deflections as well as in-plane and out-of-plane behavior are hence provided.

2. Hinge shape definitions

Various corner-filleted hinge shapes have been considered in this work. For all the shapes a constant value of the hinge aspect ratio

$$\gamma = \frac{L}{t_{\min}} \tag{1}$$

has been considered. This condition allows to take appropriately into account both the optimization constrains and the technological limits imposed by the micro-fabrication processes.

The characteristic features of the considered shapes can be summarized as:

1. *Prismatic beam hinge* of length L: idealized Euler–Bernoulli beam model that does not consider any localized stress effects – designated in the following as the *PR shape.*
2. *Circular hinge:* composed of four circular fillets (referring to Fig. 1: $a = b = r$) connected by a prismatic segment of length L_p. In this case the free parameter r ($0 < r \leqslant L/2$) can be varied to minimize the stresses occurring for a given deflection. The resulting hinge shape is indicated as the *optimized circular (OC) shape.* The particular case when $L_p = 0$ is designated as a *'pure circular (PC) hinge'* and is conventionally used as a rotational joint.

   Given their broad usage in high-precision applications, the PR and the PC hinge shapes will be used as the two limit cases to be compared with the other considered shapes.

3. *Elliptic hinge:* a variant of the circular hinge where the segment of the circle is replaced with a segment of an ellipse whose semi-axes are a and b – Fig. 1. The elliptic hinge has two free parameters that can be varied so as to minimize the resulting

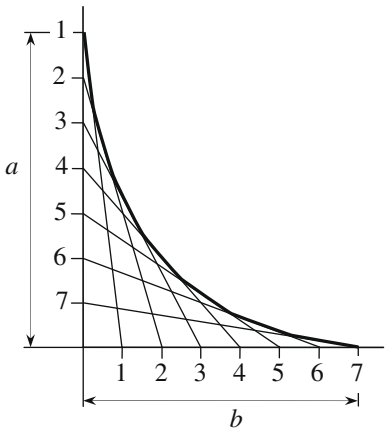

Fig. 2. GR fillet shape.

stresses: length L_p and aspect ratio b/a. The particular case of a "pure elliptic hinge", i.e. the elliptic shape with $L_p = 0$ having the b/a ratio such that, for a given rotation along the sensitive DOF, the resulting peak stresses are minimized, is indicated as the *optimized elliptical (OE) shape.*

4. *Grodzinski's (GR) hinge:* with fillets of parabolic shape [19]. The entities a and b are divided in this case into equal number of parts, but numbered in a reverse order. Homonymous numbers are connected enveloping a parabola (Fig. 2). The GR fillet has two geometrical optimization parameters: L_p and b/a. In the first instance it was assumed here that $a = b = t_{min}$, implying that $L_p = L - 2t_{min}$ and $b/a = 1$.
5. *Baud's (BS) hinge* (Fig. 3): with the fillets having the same contour as that given mathematically for an ideal, frictionless liquid, freely flowing out from an opening at the bottom of a tank [20]. This shape was thus determined from the well-known fluidodynamic similarity principles often applied to study stress concentrators, and is called as 'streamline form'. The shape was shown experimentally to produce practically no stress concentration for an axisymmetric shoulder loaded axially.

The fillet height of the BS hinge is $b = t_{min}/\pi$, while the shape of the fillet is defined by the following parametric equations (with θ defined as the slope of the tangent to the fillet with respect to coordinate x – Fig. 1 and $0 \leqslant \theta \leqslant \pi/2$):

$$x = t_{min}\left[\frac{1}{2} + \frac{1}{\pi}\left(1 - 2\sin^2\frac{\theta}{2}\right)\right] \tag{2}$$

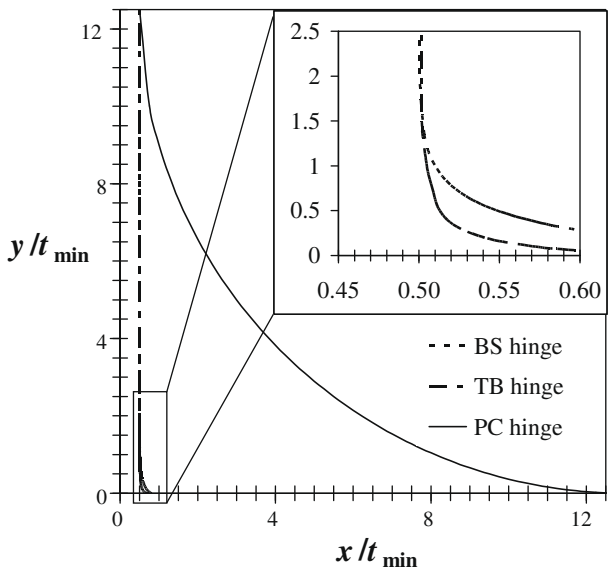

Fig. 3. Streamline (BS and TB) fillets compared to PC hinge shape.

Table 1
Geometrical parameters defining Thum's and Bautz's fillet.

$x/t_{min} = t(y)/t_{min}$	y/t_{min}
0.738	0
0.71	0.002
0.689	0.005
0.668	0.01
0.644	0.02
0.615	0.04
0.597	0.06
0.583	0.08
0.573	0.1
0.554	0.15
0.541	0.2
0.526	0.3
0.518	0.4
0.513	0.5
0.511	0.6
0.509	0.7
0.508	0.8
0.506	0.9
0.505	1
0.503	1.3
0.502	1.6
0.5	∞

$$y = \frac{t_{min}}{\pi}\left\{\ln\left[\tan\left(\frac{\theta}{2}+\frac{\pi}{4}\right)\right] - \sin\theta\right\} \tag{3}$$

The boundary conditions are:

- for $\theta = 0$: $y = 0$ and $x = t_{min}(1/2 + 1/\pi)$;
- for $\theta = \pi/2$: $y \to \infty$ and $x = t_{min}/2$.

Fillet length a would thus be infinite; by assuming a constant hinge aspect ratio γ it is, however, practically truncated to $a = (\gamma t_{min})/2 = L/2$.
The particular case of an elliptic hinge having the same fillet height b as Baud's shape, i.e. $b = t_{min}/\pi$, was also considered in this work and designated as the *EB shape.*

6. *Thum's and Bautz's (TB) hinge:* Baud's hinge, where the material in the fillet for a hinge loaded in bending was not optimally used, was optimized here empirically [20,21]. This fillet shape is defined in Table 1. Four such fillets (Fig. 3), joined so that the hinge aspect ratio is maintained constant, form the considered TB hinge.

The GR, BS and TB shapes have been obtained via stress minimization criteria for axisymmetric shoulder fillets [22]. According to Giovannozzi [23], results obtained for the axisymmetric case are also applicable to the plane case considered in this work.

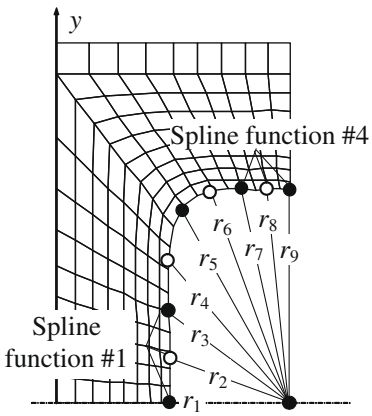

Fig. 4. Spline functions defining FO hinge shape.

Table 2
Geometrical parameters defining the considered hinge shapes.

	PR Prismatic	PC Pure circular	OC Optimized circular	OE Elliptic	EB Elliptic with BS fillet height	GR Grodzinski [19]	BS Baud [20]	TB Thum and Bautz [21]	FO Freeform
Fillets		Quarter of a circle with r = L/2	Quarter of a circle (radius $a = b = r$)	Quarter of an ellipse (semi-axes a and b)	Quarter of an ellipse with $b = t_{min}/\pi$	Parabolas as on Fig. 2, with $a = b = t_{min}$	Parametric Eqs. (2) and (3)	Table 1	Free
L_p	L	0	$L - 2r$	0	$L - 2a$	$L - 2t_{min}$	0	0	Free parameter
b/a	/	1	1	Free parameter	Free parameter	1	$2/(\gamma\pi)$		Free parameter

7. *Freeform optimized (FO) hinge shape:* the most general optimized hinge shape. In this case fillet shape is described via spline functions, following a recent original approach [18]. Spline functions are defined here as 3rd degree polynomials in a local reference frame where one of the coordinates corresponds to the middle point radius of the resulting curve (Fig. 4). Usually few (3–4) spline functions permit the notch geometry to be described quite accurately.

The comparison of geometrical parameters of all the considered hinge shapes is given in Table 2.

3. Hinge shape optimization

3.1. Optimized freeform shapes

A recently developed numerical procedure, based on the coupling of optimization algorithms with automatic FEM meshing of a parametric geometry [18], allows a very efficient nonlinear optimization of freeform flexural hinges shapes, i.e. those where geometry is defined with a large number of design parameters. In that work, however, the objective function is defined as the maximization of compliance with respect to the sensitive degree of freedom ϕ_z (Fig. 5 – an equivalent condition could be that of minimizing the volume of the material in the notch), while keeping as constraints hinge strength (stresses smaller than the allowable ones) and kinematical conditions (eccentricity e smaller than a predefined value).

In this work, for the sake of optimizing freeform shapes, a newly defined objective function is introduced: the integral of von Mises stresses along the hinge contour, which has to be maximized, i.e. referring to Fig. 5:

$$F_{FO} = \frac{1}{\int_{AB} \sigma ds} \rightarrow \min \tag{4}$$

In the considered case, making the hypothesis of plane stress, von Mises stresses reduce to stress σ_t, while σ_n and τ_{nt} vanish (Fig. 6). The constraint of keeping the stresses smaller than the allowable ones is still kept.

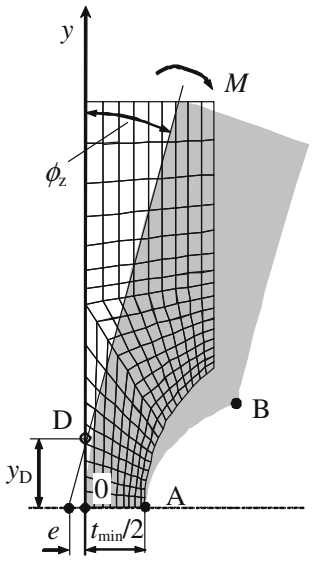

Fig. 5. FO hinge model used in the optimization procedure.

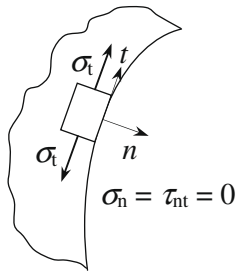

Fig. 6. Stress state in hinge contour.

This new approach permits localized effects of hinge shape modifications to be taken into account better. The rate of convergence and the robustness of the optimization process are thus improved, while making the procedure much more sensitive to design goals. What is more, this new formulation of the optimization procedure allows an increased number of spline functions to be used while preserving the stability of the calculation. This results in a far better description of the obtained FO shape.

In the optimization of flexural hinge shapes it is important to take into consideration parasitic motions, i.e. deflections along the secondary degrees of freedom, but also technological constraints that impose strict limits on the shapes which can be practically produced. In the optimization algorithm used in this work, the kinematical constraint defined by eccentricity e is hence replaced by a constraint on the value of the hinge aspect ratio $\gamma = L/t_{min}$. This parameter allows the technological limits imposed by today's precision manufacturing processes to be taken into account. This is further supported by the direct correlation between eccentricity and hinge length proven in [18].

The case of hinges loaded with a pure couple M at the free end is considered. The conditions of symmetry and anti-symmetry enable only one quarter of the hinge to be modeled (Fig. 5). Devices of relatively small width w (see Fig. 1) are taken into account, i.e. plane stress conditions are used in the model. In cases where this boundary condition would not be valid, bending stiffening from E to $E/(1-\nu^2)$ would have to be taken into account [24], i.e. the respective transition from plane stress to plane strain conditions would have to be considered [25]. As noted recently by Angeli et al. [26], it is important to remark that this transition also depends on loading conditions, so that for increasing loads every beam can present a plate-like behavior.

3.2. Predefined shapes

In the case of hinges of predefined (circular and elliptic) shapes, the number of design parameters is reduced to one or two, e.g. the semi axes a and b of the elliptic fillet shape. Optimization therefore reduces to the following procedure: for an imposed hinge deflection by a constant angle ϕ_z, the search of the values of the free design parameters up to the point when the maximal stress occurring in the hinge is minimized

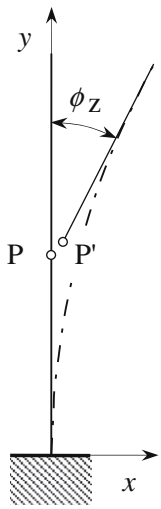

Fig. 7. Schematic representation of parasitic shift PP'.

$$F_i = \sigma_{max} \rightarrow \min \tag{5}$$

is performed.

The choice of imposing a deflection angle instead of loading the hinge with a constant couple M, as was done in the case of FO shape optimization, is made possible by employing geometric similitude (same shapes are dimensionally scaled). In fact, by imposing geometric similarity via the assumption of a constant hinge aspect ratio γ, equal deflection angles for structures made of the same material result in stresses of equal magnitude.

3.3. Shape comparison

To compare initially the above-defined shapes, a constant hinge aspect ratio $\gamma = 25$ is assumed. Such a value is chosen so as to emphasize the parasitic shifts, while minimizing shear effects. On the thus-obtained optimal shapes the calculation of hinge compliances as well as a geometrically nonlinear (large deflections) FEM determination of the values of the parasitic shifts PP' (Fig. 7) is performed. Point P is coincident here with the middle of the hinge. In an ideal joint P would be the fixed point around which rotation occurs. For slender hinges, however, this point moves as the beam deflects, hence inducing deviations from ideal pivot kinematics and assuming the position of point P' linked to the mobile element. The parasitic shift PP' is physically equal to eccentricity e [18] as shown in Fig. 5. In the nonlinear FEM calculations of the parasitic shift, anti-symmetry conditions are not applicable any more and half of the hinge has to be modeled.

4. Obtained results

4.1. Results and discussion for $\gamma = 25$

The FO shape for the assumed hinge aspect ratio $\gamma = 25$ resulting from the above optimization procedure is very similar to the TB shape obtained empirically for bulky axisymmetric shoulder fillets (Fig. 8). It was established that for $\gamma \geqslant 2.5$ the FO shape does not depend on γ, i.e. hinge shapes for hinge lengths $L \geqslant 2.5t_{min}$ are obtained simply by adding a prismatic section of suitable length L_p. The determined FO fillet shape is in this regard an 'absolute optimum'. On the other hand, by reducing the value of γ below 2.5, compliance is greatly reduced, which conflicts with the objective of increasing the hinge working range. The FO fillet shape for any $\gamma \geqslant 2.5$ can thus be approximated by the values given in Table 3.

The optimization of conventional shapes by using the outlined procedure has given as optima:

- OC shape with $r = 1.3818t_{min}$,
- OE shape with $b/a = 0.0314$, and
- EB shape with $a = 0.058L$.

It is worth noting here that in the case of elliptic and circular hinge shapes, given the elongated geometry ($\gamma = 25$), in a rather wide range of the considered geometrical parameters (semi-axes a and b or fillet radius r, respectively), the value of

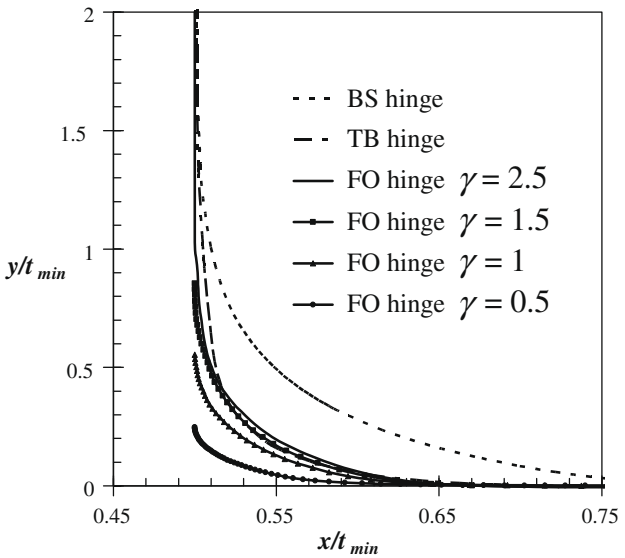

Fig. 8. FO, BS and TB shapes.

Table 3
Geometrical parameters defining the FO fillet shape for any $\gamma \geqslant 2.5$.

$x/t_{min} = t(y)/t_{min}$	y/t_{min}
1.155	0
0.83	0
0.778	−0.005
0.751	−0.006
0.695	−0.002
0.666	0.003
0.693	0.014
0.615	0.037
0.596	0.068
0.579	0.105
0.564	0.145
0.552	0.189
0.544	0.223
0.531	0.296
0.521	0.369
0.514	0.444
0.509	0.518
0.506	0.591
0.503	0.732
0.501	0.932
0.5	1.155
0.5	∞

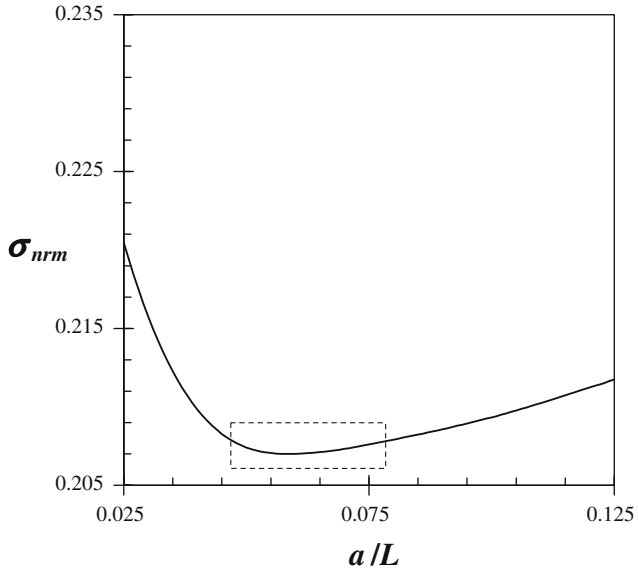

Fig. 9. Variation of normalized stress vs. parameter a/L for an elliptic hinge. In the indicated zone several minima can occur. Similar behavior also occurs for parameter b/L.

the obtained stresses differs only slightly from the absolute optimum (Fig. 9). This implies the need to use very fine FEM meshes in the fillet region, with a resulting increment in the computational times.

Indicating with E the modulus of elasticity and with σ_{max} the maximum stress occurring in the hinge, the following normalized parameters, i.e. normalized stresses, compliances and parasitic shifts, are introduced:

$$\sigma_{nrm} = \frac{\sigma_{max}}{E\phi_z} \ [\text{rad}^{-1}] \tag{6}$$

$$C_{nrm} = \frac{Ewt_{min}^3\phi_z}{ML} \ [\text{rad}] \tag{7}$$

$$\delta_{nrm} = \frac{PP'}{L} \tag{8}$$

To compare the thus-obtained values with those obtained for the PC hinge, the following ratios are defined (index "*i*" indicates the various fillets):

$$K_\sigma = \frac{\sigma_{\mathrm{nrm\_PC}}}{\sigma_{\mathrm{nrm\_}i}} \tag{9}$$

$$K_C = \frac{C_{\mathrm{nrm\_}i}}{C_{\mathrm{nrm\_PC}}} \tag{10}$$

$$K_\delta = \frac{\delta_{\mathrm{nrm\_}i}}{\delta_{\mathrm{nrm\_PC}}} \tag{11}$$

K_σ represents the ratio of the maximal stresses occurring, respectively, in the PC and in the considered hinge shape for a given deflection angle. K_C is the compliance ratio giving the relative deflection of the considered shape for a given load. The ratio between K_σ and K_C gives a direct indication of stress concentration. In fact, for hinges of the same material and the same characteristic geometric parameter γ, it will be:

$$\frac{K_\sigma}{K_C} = \frac{\frac{\sigma_{\mathrm{max\_PC}}}{E\phi_{z\_PC}}}{\frac{\sigma_{\mathrm{max\_}i}}{E\phi_{z\_}i}} \frac{\frac{Ew_{PC}t^3_{\mathrm{min\_PC}}\phi_{Z\_PC}}{M_{PC}L_{PC}}}{\frac{Ew_it^3_{\mathrm{min\_}i}\phi_{z\_}i}{M_iL_i}} = \frac{\sigma_{\mathrm{max\_PC}}\phi_{z\_}i}{\sigma_{\mathrm{max\_}i}\phi_{z\_PC}} \frac{M_iw_{PC}t^2_{\mathrm{min\_PC}}\phi_{z\_PC}}{M_{PC}w_it^2_{\mathrm{min\_}i}\phi_{z\_}i} = \frac{\frac{\sigma_{\mathrm{max\_PC}}}{\sigma_{\mathrm{n\_PC}}}}{\frac{\sigma_{\mathrm{max\_}i}}{\sigma_{\mathrm{n\_}i}}} = \frac{\alpha_{\mathrm{k\_PC}}}{\alpha_{\mathrm{k\_}i}} = K^*_\sigma \tag{12}$$

where $\sigma_{\mathrm{n\_PC}}$, $\sigma_{\mathrm{n\_}i}$, $\alpha_{\mathrm{k\_PC}}$ and $\alpha_{\mathrm{k\_}i}$ are, respectively, the nominal stresses and the stress concentration factors for the circular and the considered hinge shapes. K^*_σ represents the relative stress concentration factor. Finally, K_δ represents the relative parasitic shift amplitude.

Fig. 10 shows the values of K_σ, K^*_σ, K_C and K_δ for the considered shapes when $\gamma = 25$. The following conclusions can hence be drawn:

- The freeform optimized (FO) shape provides results that are equivalent in terms of strength and compliance to those of a prismatic spring with no stress concentrations and presents thus virtually no room for further improvement.
- In terms of strength, the BS and EB shapes also provide results close to those of the PR shape, whereas the optimal elliptic (OE) shape is clearly the worst.
- Considering compliances, the "ranking" in terms of decreasing compliance is: BS, FO, EB, TB, OC, GR and OE.
- In terms of stress concentration, results obtained for all the shapes clearly indicate that there is virtually none, i.e. that the respective stress concentration factors tend to be equal to 1.
- Given the relatively large γ value, the normalized parasitic shift δ_{nrm} as the function of deflection ϕ_z is basically the same for all shapes but for the conventional circular PC shape, and equal to that of the PR shape.
- On the other hand, if the dependence of δ_{nrm} on the normalized load $ML/(Ewt^3_{\mathrm{min}})$ is considered for equal loading conditions on all hinges, marked differences can be observed. Fig. 10 shows results in terms of relative parasitic shift based on the normalized parasitic shift calculated for the load that produces $\phi_z = 0.17$ rad (10°) for the PC shape (deflections of

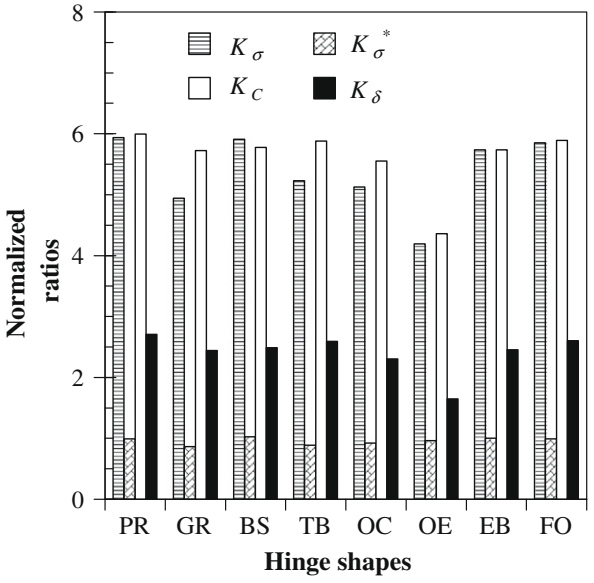

Fig. 10. Normalized ratios K_σ, K^*_σ, K_C and K_δ vs. hinge shape for $\gamma = 25$.

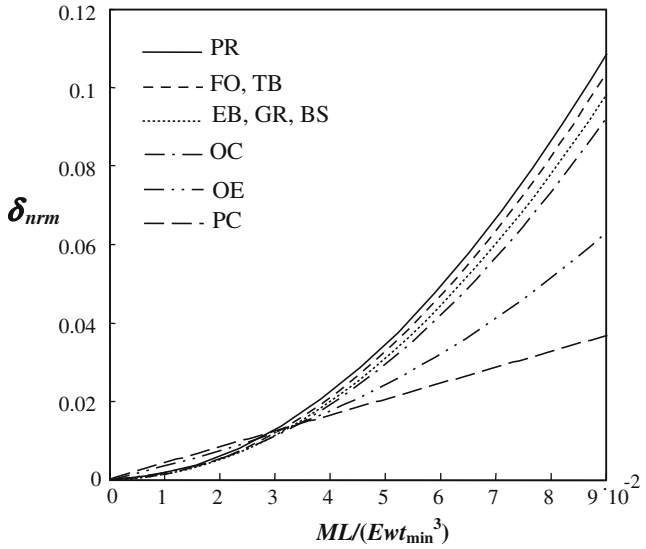

Fig. 11. δ_{nrm} vs. normalized load for considered hinge shapes with $\gamma = 25$.

almost 1.05 rad (60°) are obtained with the same load in the case of the most compliant shapes). It is thus evident that improvement in terms of strength and compliance is inversely proportional to parasitic shift magnitude.

- For the most compliant shapes (streamline and optimized ones), however, the load to be applied for a certain deflection is much smaller than that applied in the case of the PC shape. This is especially relevant for loads that in the PC shape produce rotations smaller than ca. 0.09 rad (5°). For these loads δ_{nrm} of the most compliant hinge shapes is even smaller than that of the PC shape. For larger loads this is not true any more, since normalized compliance of these shapes grows exponentially (Fig. 11).

4.2. Results and discussion for different hinge aspect ratios and influence of secondary loads

The same procedure as outlined above for the hinge aspect ratio $\gamma = 25$ was also extended to other values of γ (only some characteristic values are reported in this work). In this case, as stated above, FO shape remains the same, except for the length of the prismatic section L_p, while the OC, EB and OE dimensions had to be optimized again. The resulting geometric parameters are given in Table 4 in terms of the adopted shape normalization characteristics. On the other hand, the remaining shapes (the streamline ones, i.e. those obtained empirically) were shortened while keeping the same fillet section.

The influence of hinge aspect ratio on the characteristic strength, compliance and parasitic ratios defined in Eqs. (9)–(12) can be summarized as:

- For decreasing values of γ, the values of normalized stresses increase, while hinge strength expressed by K_σ tends to become closer to that of the PC hinge. However, even for the smallest considered aspect ratio ($\gamma = 5$), optimized shapes still allow a significant improvement in terms of strength. This is due to compliance reduction. In fact, when K_σ^* is considered, no significant differences can be observed when γ is varied. In Fig. 12 the respective values for the FO shape are shown.
- The influence of the hinge aspect ratio γ on the compliance ratio K_C, shown in Fig. 12 for the FO shape, has a similar tendency also for the other hinge shapes and is characterized by the fact that, for a decreasing γ, K_C decreases with a rate roughly proportional to γ.
- For different values of the hinge aspect ratio, parasitic shifts show a pattern similar to that shown in Fig. 11.

Table 4
Geometrical parameters of optimized shapes for different aspect ratios γ.

	OC	OE	EB
$\gamma = 5$	$r = 0.59t_{min}$	$b/a = 0.103$	$a = 0.18L$
$\gamma = 10$	$r = 0.825t_{min}$	$b/a = 0.062$	$a = 0.12L$
$\gamma = 25$	$r = 1.3818t_{min}$	$b/a = 0.0314$	$a = 0.058L$

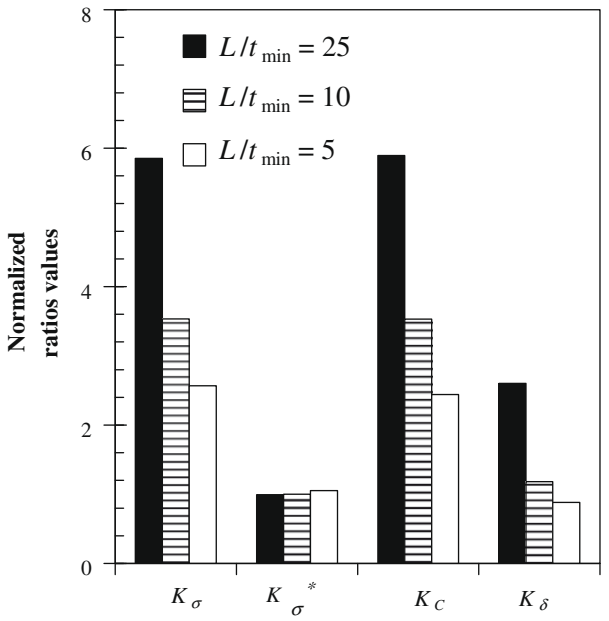

Fig. 12. Values of normalized ratios K_σ K_σ^*, K_C and K_δ for the FO hinge shape and different hinge aspect ratios γ.

On the thus-obtained optimized shapes, a comparison of transversal bending (out of hinge plane, i.e. around x axis) and axial (along y axis) stresses and compliances was done. For all the considered aspect ratios γ, hinge shape was shown to have a very small influence on axial and transversal compliances (always within ±5% for all shapes but for the OE shape, which is clearly worse than the others). On the other hand, the influence of the shape on the relative stress concentration factor K_σ^* is significant both in transversal and in axial directions (Figs. 13 and 14, respectively). It is worth noting that in this case K_σ^* is relevant for the determination of strength, as along the secondary DOFs only the behavior of the hinge for a given load is significant.

In terms of decreasing strength in transversal bending, the shapes can be ordered as: BS, GR, OC, EB, TB, FO and OE. In the axial loading case, the order is: GR, BS, OC, EB, TB, FO and OE. As shown in Figs. 13 and 14, aspect ratio γ has a small influence on these results.

Thus, hinge shapes that are most compliant around the primary DOF (FO and TB) tend to exhibit greater stress concentrations than some of the other ones. This is particularly relevant since it has been observed already that intermediate shapes (i.e. between the best ones in terms of strength along the sensitive DOF and those exhibiting the worst results along this

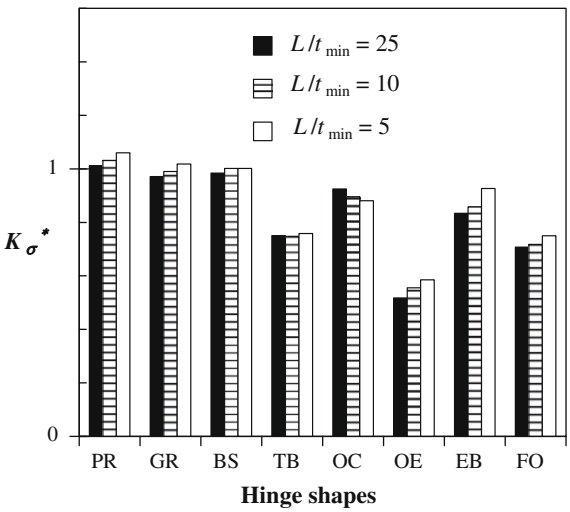

Fig. 13. Relative stress concentration factors for transversal bending.

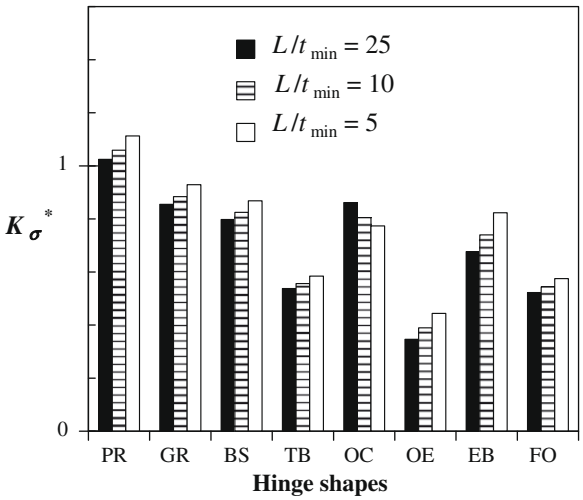

Fig. 14. Relative stress concentration factors for axial loading.

DOF) tend to produce smaller parasitic shifts than the rotationally most compliant ones. The optimal shape to be used will thus depend on a trade-off between the possibility to increase strength and compliance of the notch along the sensitive DOF on one hand, and the parasitic shifts along the primary DOF and the stresses along the secondary DOFs on the other hand.

Given these considerations, it can be concluded that the FO and TB shapes will be the preferred choice only when the goal is compliance maximization along the primary hinge DOF. The GR, BS and the optimized OC and EB shapes will be the favorite choice when both the entity of the parasitic shifts with respect to the primary DOF, and stress-concentration effects in axial and transversal directions, are important for the considered application.

5. Conclusions

The nonlinear parametric optimization of predefined and freeform flexural hinge shapes, as well as the comparison among these and shapes obtained via stress minimization criteria for shoulder fillets was performed in terms of compliance, strength, stress concentration factors and parasitic shifts. It was thus shown that, for the freeform optimized shape, hinge relative dimensions do not have an influence on the obtained solution. In the case of predefined optimized shapes, a variation of relative dimensions induces a change in the fillet shape. Moreover, the freeform shape provides in terms of strength and compliance results that are equivalent to those of a prismatic spring and presents thus virtually no room for further improvement. For all the considered cases, improvement in terms of strength and compliances is, however, inversely proportional to parasitic shift magnitude. The analysis of transversal and axial compliances and stress concentration factors of the obtained optimized shapes shows that the shapes that are most compliant around the primary degree of freedom tend to exhibit greater stress concentrations along the secondary DOFs. Some of the considered shapes result, however, in a good compromise. Far smaller stresses than those in conventional hinge shapes, but also smaller parasitic shifts along the primary DOF and smaller stress concentrations along the secondary DOFs, are hence obtained. In any case, optimization of hinge shapes permits a strong improvement of their behavior and should thus be adopted as a standard design procedure for compliant devices based on flexures.

Acknowledgments

This work was supported by the "*Ultra-high precision compliant devices for micro and nanotechnology applications*" project supported by the Croatian Ministry of Science, Education and Sports, the "*Theoretical and experimental analysis of compliant mechanisms for micro- and nano-mechanical applications*" project of the Italian Ministry of University and Research and the "*A Stronger Europe with MIcro- and Nanotechnologies (SEMINA)*" project in the frame of the SCOPES program of the Swiss National Science Foundation.

The authors wish to thank S. Henein for some useful ideas in the initial phases of the work on the described topics.

References

[1] B. Bhushan (Ed.), Springer Handbook of Nanotechnology, Springer, Berlin, Germany, 2004.
[2] S. Henein, I. Kjelberg, S. Zelenika, Flexible bearings for high-precision mechanisms in accelerator facilities, in: Proceedings of NANOBEAM 2002 – 26th Advanced ICFA Beam Dynamics Workshop on Nanometre-Size Colliding Beams, Lausanne, Switzerland, 2002, pp. 103–110.
[3] L.L. Howell, Compliant Mechanisms, John Wiley & Sons, New York, NY, USA, 2001.

[4] N. Maluf, An Introduction to Microelectromechanical Systems Engineering, Artech House Publishers, Boston, MA, USA, 2000.
[5] D. Shu, Th.S. Toellner, E.E. Alp, Modular overconstrained weak-link mechanism for ultraprecision motion control, Nuclear Instruments and Methods in Physics Research A 467–468 (1) (2001) 771–774.
[6] A.H. Slocum, Precision Machine Design, Society of Manufacturing Engineers, Dearborn, MI, USA, 1992.
[7] N. Lobontiu, Compliant Mechanisms: Design of Flexure Hinges, CRC Press, Boca Raton, FL, USA, 2002.
[8] S.T. Smith, Flexures – Elements of Elastic Mechanisms, Gordon and Breach Science Publishers, Amsterdam, Netherlands, 2000.
[9] S. Awtar, Synthesis and Analysis of Parallel Kinematic XY Flexure Mechanisms, Ph.D. Thesis, MIT, Massachusetts, MA, USA, 2004.
[10] R.J. Chang, H.S. Wang, Y.L. Wang, Development of mesoscopic polymer gripper system guided by precision design axioms, Precision Engineering 27 (2003) 362–369.
[11] S.-C. Chen, M.L. Culpepper, Design of a six-axis micro-scale nanopositioner – μHexFlex, Precision Engineering 30 (2006) 314–324.
[12] M.L. Culpepper, G. Anderson, Design of a low-cost nano-manipulator which utilizes a monolithic, spatial compliant mechanism, Precision Engineering 28 (2004) 469–482.
[13] S. Henein, U. Frommherz, R. Betemps, H. Kalt, U. Ellenberger, U. Flechsig, J. Raabe, Mechanical design of a spherical grating monochromator for the microspectroscopy beamline PolLux at the swiss light source, in: American Institute of Physics Conference Proceedings 879 – Ninth International Conference on Synchrotron Radiation Instrumentation SRI 2006, Daegu, Exco, Korea, 2007, pp. 643–646.
[14] T.C. Tseng, D.J. Wang, S.Y. Perng, C.K. Kuan, J.R. Lin, S.H. Chang, C.T. Chen, Development of a novel aspherical mirror bender for an active grating, Journal of Synchrotron Radiation 10 (2003) 450–454.
[15] Q. Yao, J. Dong, P.M. Ferreira, A novel parallel-kinematics mechanisms for integrated, multi-axis nanopositioning Part 1: kinematics and design for fabrication and Part 2: dynamics, control and performance analysis, Precision Engineering 32 (2007) 7–33.
[16] J.M. Paros, L. Weisbord, How to design flexure hinges, Machine Design 37 (1965) 151–156.
[17] S.T. Smith, V.G. Badami, J.S. Dale, Y. Xu, Elliptical flexure hinges, Review of Scientific Instruments 68 (1997) 1474–1483.
[18] F. De Bona, M.Gh. Munteanu, Optimized flexural hinges for compliant micromechanisms, Analog Integrated Circuits and Signal Processing 44 (2) (2005) 163–174.
[19] P. Grodzinski, Investigations on shaft fillets, Engineering 152 (1941) 321–324.
[20] R.V. Baud, Beiträge zur Kenntnis der Spannungsverteilung in prismatischen und keilförmigen Konstruktionselementen mit Querschnittübergängen, Ph.D. Thesis, EHT Zurich, Switzerland, 1934.
[21] A. Thum, W. Bautz, Der Entlastungübergang – Günstigste Ausbildung des Überganges an abgesetzten Wellen u. dgl., Forschung Ingenieurwesen 6 (1934) 269–273.
[22] W.D. Pilkey, Peterson's Stress Concentration Factors, second ed., John Wiley & Sons, New York, NY, USA, 1997.
[23] R. Giovannozzi, Costruzione di macchine, vol. I, Patron editore, Bologna, Italy, 1965.
[24] D.G. Ashwell, The anticlastic curvature of rectangular beams and plates, Engineering (1947) 708–715.
[25] B. Zettl, W. Szyszkowski, W.J. Zhang, Accurate low DOF modeling of a planar compliant mechanism with flexure hinges: the equivalent beam methodology, Precision Engineering 29 (2005) 237–245.
[26] P. Angeli, F. De Bona, M.Gh. Munteanu, Flexural stiffness evaluation of leaf spring compliant mechanisms, in: Proceedings of the II International Conference on Computational Mechanics and Virtual Engineering – COMEC 2007, Brasov, Romania, 2007, pp. 269–274.